



# Tissue fluids in microchannel subjected to an externally applied electric potential

Vincent C. Huang and Tony W.H. Sheu

*Department of Engineering Sciences and Ocean Engineering,  
National Taiwan University, Taipei, Taiwan*

Received 5 March 2007  
Revised 17 October 2007  
Accepted 19 November 2007

## Abstract

**Purpose** – The purpose of this paper is to describe the development of an electroosmotic dynamic model to simulate the transport phenomena in association with the electric therapy in modern medicine.

**Design/methodology/approach** – The present study builds a new model by employing SUPG finite element method to solve the electroosmotic transport equation in microchannels of human body.

**Findings** – The present electroosmotic finite element analysis demonstrated that the electric treatment has a better curative effect.

**Research limitations/implications** – The governing electric field equations for tissue fluids in microchannel include the Laplace equation for the effective electrical potential and the Helmholtz equation for the electrical potential established in the electric double layer (EDL). The transport equations governing the hydrodynamic field variables include the mass conservation equation for the electrolyte and the equations of motion for the incompressible charged fluids subject to an electroosmotic body force.

**Practical implications** – The phenomena of microchannels are dominated by elliptic equations, Laplace, Helmholtz and diffusion equations (Navier Stokes equations at  $Re = 0.0259$ ). These governing equations explain why the reaction of electric treatment is very fast, even immediate.

**Originality/value** – The analysis of the coupled hydrodynamic and electrical fields, the externally applied electric potential has been shown to be an aid to accelerate the tissue fluid due to the formation of an EDL. Interaction of plasma and tissue fluids in human body is also revealed.

**Keywords** Finite element analysis, Hydrodynamics, Flow, Human physiology, Modelling

**Paper type** Research paper

## 1. Introduction

The length scales in tissue fluids are slightly larger than  $10\ \mu$ . Owing to the large surface-to-volume ratio in microchannels, the liquid subjected to an externally applied electrical field may be greatly influenced by the interfacial effect due to the formation of an electric double layer (EDL). Study of the applied electric field interacted with the charged fluids near the channel walls or around the suspended charges becomes essential. In other words, to acquire knowledge regarding the coupling mechanism of ion flow and electric fields turns out to be an academic subject worthy of an intensive exploration in the field of electrohydrodynamics.

On the charged surface, which is in contact with an electrolyte, EDL consists of a compact layer of immobile balancing charges and a diffuse layer of mobile ions. The thickness of the counter-ion shielding layer can be characterized by its Debye length, which typically has a length of 10 nm or less. The interface between the compact (or stern) and diffuse layers, in which the liquid velocity is zero under the zero pressure gradient condition, is known as the shear plane. In the diffuse layer, the excess counter



ions can be transported by an externally applied force. This electroosmotic phenomenon was firstly observed by Reuss (1809). The formation of the resulting bulk flow is now known to be the consequence of electroosmosis force since the moving ions can drag their surrounding fluids by virtue of the fluid viscosity.

Subsequent to the mathematical theory proposed by Wiedemann (1852), the progress towards investigating the electroosmotic flows in complex microfluidic networks for loading, mixing, and flushing purposes has been considerable (Sinton *et al.*, 2002; Lin *et al.*, 2002; Chang and Yang, 2004; Liu *et al.*, 2004). Owing to the emerging lab-on-a-chip microfluidic devices, numerous experimental and computational studies have been carried out for enhancing our understanding of the electroosmotic phenomena in microchannels. Most of the pervious studies have been denoted to the exploration of hydrodynamic behaviors for various industrial applications (Mala *et al.*, 1997; Patankar and Hu, 1998; Stroock *et al.*, 2002; Chen *et al.*, 2004).

Electro-treatments have long been known to be effective in relieving the pain (Mao *et al.*, 1980; Han *et al.*, 1983; Romita *et al.*, 1997; Ulett *et al.*, 1998; Wan *et al.*, 2001; Huang *et al.*, 2002). Bensoussan (1991) found that human acupuncture points are usually located near the blood vessels, nerves and receptors, lymphatics. Tiberiu and Gheorge (1981) used the ions of radioactive isotope, injected into the acupuncture points, and found that ions are migrated along the gaps of myo-fiber to form a route as meridian in Chinese medicine. However, very little attention has been paid to the study of conductive tissue fluids in human microchannels. This study is aimed to build an electroosmosis model to simulate the interaction of blood and tissue fluid under the action of physiological acupuncture.

The rest of this paper is organized as follows. Section 2 presents the electrohydrodynamic governing equations. This is followed by briefly presenting the finite element model employed for solving the EOF equations given in Section 2 and the code validation in Section 4. Section 5 describes the model problem and discusses the predicted results in details. Finally, some conclusions will be drawn in Section 6.

## 2. Governing equations

In the physical domain  $\Omega$ , the working equations adequate for the current electrohydrodynamic study will be described. The Laplace equation given below is used to model the externally applied potential ( $\varphi$ )

$$\nabla^2 \varphi = 0 \quad (1)$$

For the tissue fluid with ions described by the Boltzmann distribution, the  $\zeta$  potential  $\Psi$  in the EDL can be modeled by the following Helmholtz equation:

$$\nabla^2 \psi = \frac{1}{\lambda_D^2} \psi \quad (2)$$

In the above, the Debye and Hückel (1923) length  $\lambda_D$ :

$$\left( \equiv \left( \frac{k_b T \varepsilon}{e^2 \sum_i n_{i0} z_i^2} \right)^{1/2} \right)$$

is equal to  $8.93 \times 10^{-7}$  m. Note that  $k_b$  is known as the Boltzmann constant,  $\varepsilon$  the permittivity of the buffer solution,  $T$  the absolute temperature,  $e$  the elementary charge,

$n_{i0}$  the ion density bulk solution, and  $z_i$  the valence of the ion. Finally, the momentum equation subjected to the externally applied electro-kinetic body force can be expressed as follows (Jahrul and John, 2002):

$$u \cdot \nabla u = -\frac{1}{\rho} \nabla P + \mu \nabla^2 u + \frac{\varepsilon}{\rho \lambda_D^2} \psi \nabla(\varphi + \psi) \quad (3)$$

where  $u$  is the velocity,  $p$  the pressure,  $\mu$  the dynamic viscosity (blood:  $\mu = 3.0 \times 10^{-3}$  Pa s; tissue fluid:  $\mu = 1.2 \times 10^{-3}$  Pa s) (Fung, 1997) and  $\rho$  the density ( $\rho = 1,057$  kg/m<sup>3</sup> for the blood;  $\rho = 1,035$  kg/m<sup>3</sup> for the tissue fluid) (Fung, 1997). For the investigated incompressible fluid flow, the equation for the conservation of mass is given by:

$$\nabla \cdot u = 0 \quad (4)$$

### 3. Finite element model for the transport equations

Within the streamline upwind Petrov Galerkin finite element framework, the weighting function  $W$  is given by:

$$W_i = N_i + B_i \quad (5)$$

where  $N_i$  is the shape function. In the above, the biased weighting function  $B_i$  is given by:

$$B_i = \tau N_i \tilde{V}_i^k \frac{\partial N_i}{\partial x^k} \quad (6)$$

where  $\tau$  determines the degree of upwinding (Sheu *et al.*, 1995; Wang and Sheu, 1997; Sheu and Chen, 1999; Sheu and Tsai, 1999). To solve the incompressible electroosmotic transport equations shown in Section 2, the bi-quadratic shape function ( $N_i, i = 1 \sim 9$ ) for the velocity vector field and the bi-linear shape function ( $M_i, i = 1 \sim 4$ ) for the pressure unknown will be employed so that the required Ladysenskaja-Babuska-Brezzi condition (Ladyshenskaya, 1969) for the chosen set of primitive variables is satisfied (Sheu *et al.*, 1995). The resulting weak solutions  $u_j, v_j$  and  $p_j$  for equations (3) and (4) can be calculated from the matrix equation given by:

$$\left[ \int_{\gamma^h} \begin{bmatrix} C_{ij} & 0 & -M_j \frac{\partial N_i}{\partial x} + B_i \frac{\partial M_j}{\partial x} \\ 0 & C_{ij} & -M_j \frac{\partial N_i}{\partial y} + B_i \frac{\partial M_j}{\partial y} \\ M_i \frac{\partial N_j}{\partial x} & M_i \frac{\partial N_j}{\partial y} & 0 \end{bmatrix} d\Omega^h \right] \begin{pmatrix} u_j \\ v_j \\ p_j \end{pmatrix} = \int_{\gamma^h} \begin{pmatrix} D_j \\ D_j \\ 0 \end{pmatrix} d\Omega^h \quad (7)$$

where:

$$C_{ij} = (N_i + B_i) \left( N_j \tilde{V}_j^k \right) \cdot \frac{\partial N_j}{\partial x^k} + \mu \frac{\partial N_i}{\partial x^k} \frac{\partial N_j}{\partial x^k} - B_i \frac{\partial^2 N_j}{\partial x^k \partial x^k}$$

and  $D_j = (N_i + B_i) \frac{\varepsilon}{\rho \lambda_D^2} \psi_i \frac{\partial N_i}{\partial x^k} \varphi_i \cdot$

Since the differential equations for modelling the respective applied electric potential and  $\zeta$  potential in equations (1) and (2) are classified to be elliptic, their resulting Galerkin equations can be expressed as:

$$\int_{\Omega^h} \left( \frac{\partial N_i}{\partial x} \frac{\partial N_j}{\partial x} + \frac{\partial N_i}{\partial y} \frac{\partial N_j}{\partial y} \right) \varphi d\Omega^h = 0 \quad (8)$$

$$\int_{\Omega^h} \left( \frac{\partial N_i}{\partial x} \frac{\partial N_j}{\partial x} + \frac{\partial N_i}{\partial y} \frac{\partial N_j}{\partial y} + \frac{1}{\lambda_D^2} \right) \psi d\Omega^h = 0 \quad (9)$$

In this paper, the frontal direct solver will be employed to calculate the solutions from the respective matrix equations given in equations (7)-(9).

#### 4. Verification study

For the sake of verification, the analytical problem of Prashanta and Ali (2001), subjected to the boundary conditions schematic in Figure 1, is chosen for comparing the predicted electroosmotic/pressure mixed flow solution with the exact solution in the straight channel, which has a dimensionless height of 1. For the flow in the channel with a width, which is much smaller than the channel length, it is assumed to be steady and fully developed. Given the dimensionless electroosmotic potential  $\Psi$ , the predicted  $\zeta$  potential in Figure 2 is shown to have a good agreement with the analytic solution given by Prashanta and Ali (2001). The predicted velocity profiles shown in Figure 3 are also seen to compare fairly well with the exact velocity distributions under the different prescribed inlet pressure values.

#### 5. Discussion of results

Tissue fluid and blood flows can interact with each other through the activities amongst the myo-fibers, micro-vessels, lymphatic and nerves. To highlight the dynamical behaviours, both tissue fluids and blood fluids will be taken into account. According to the physiological sizes and coefficients of microcirculation given in Fung (1997) and Valtin and Schafer (1995), the relationship between the arteriole and venule vessels and the tissue fluid is clearly shown in Figure 4. The pressure and velocity in the arteriole are both specified to have larger magnitudes than those in the venule vessels and the tissue fluid channel. The venule vessels have been specified to have the negative pressure boundary values, while the tissue fluid path is assumed to have the zero pressure at the outlet. The applied boundary conditions schematic in Figure 4 are summarized as below (Valtin and Schafer, 1995):

Capillary inlet (arteriole end):

$$\varphi = 50 \text{ V}, \frac{\partial \psi}{\partial x} = 0 \text{ V/m}, \frac{\partial u}{\partial x} = \frac{\partial v}{\partial x} = 0 \text{ sec}^{-1}, P = 20 \text{ mmHg}. \quad (10)$$

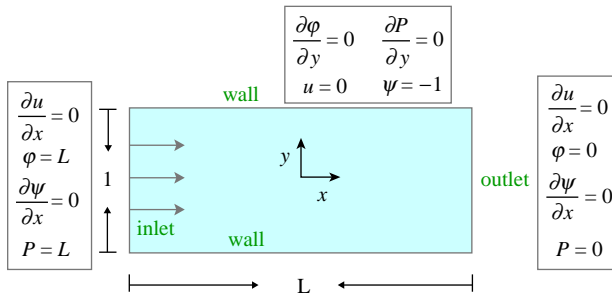


**Figure 1.**  
The specified boundary  
conditions for the  
analytical test problem

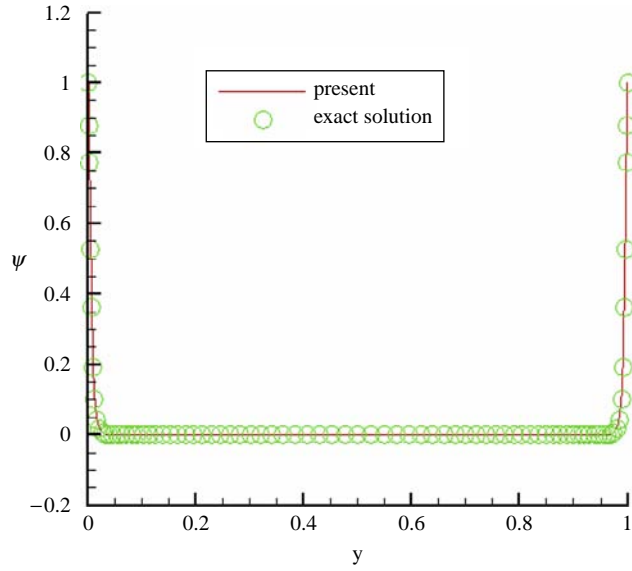


**Figure 2.**  
Comparison of the predicted and analytical  $\zeta$  at different values of  $y$

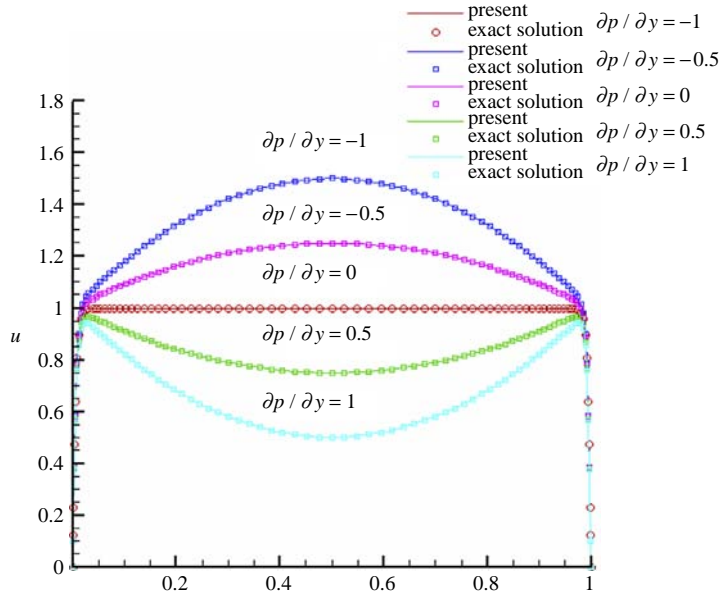


**Figure 3.**  
Comparison of the predicted and analytical velocity profiles at different values of  $\partial p / \partial y$

Capillary outlet (venule end):

$$\varphi = 0 \text{ V}, \frac{\partial \psi}{\partial x} = 0 \text{ V/m}, \frac{\partial u}{\partial x} = \frac{\partial v}{\partial x} = 0 \text{ sec}^{-1}, P = -10 \text{ mmHg.} \quad (11)$$

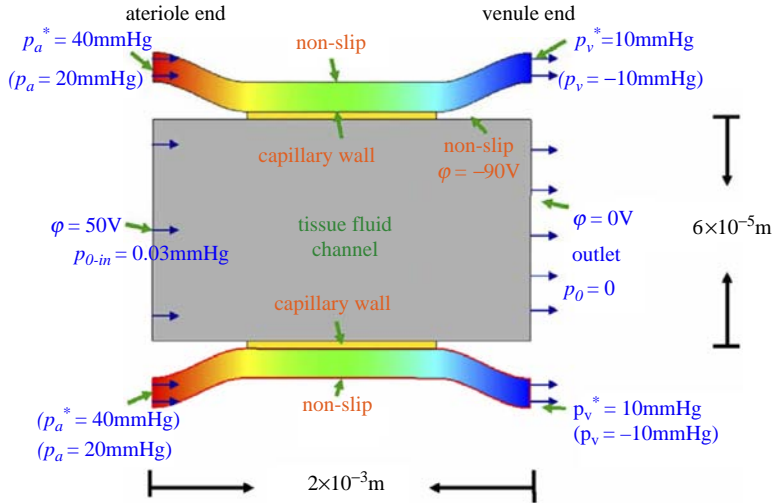


**Figure 4.** Schematic of the tissue fluid channel and the capillaries considered in the proposed electroosmosis transport model

Tissue fluid at the channel inlet:

$$\varphi = 50 \text{ V}, \frac{\partial \psi}{\partial x} = 0 \text{ V/m}, \frac{\partial u}{\partial x} = \frac{\partial v}{\partial x} = 0 \text{ sec}^{-1}, P = 0.03 \text{ mmHg}. \quad (12)$$

Tissue fluid at the channel outlet:

$$\varphi = 0 \text{ V}, \frac{\partial \psi}{\partial x} = 0 \text{ V/m}, \frac{\partial u}{\partial x} = \frac{\partial v}{\partial x} = 0 \text{ sec}^{-1}, P = 0 \text{ mmHg}. \quad (13)$$

Walls of capillary and tissue fluid:

$$\frac{\partial \varphi}{\partial x} = 0 \text{ V/m}, \psi = 0.09 \text{ V}, u = v = 0 \text{ m/sec} \quad (14)$$

The current study employs 48,389 nodal points to generate the mesh shown in Figure 5. The mesh densities have been kept increasing until the computed solutions shown in Figure 6 and tabulated in Table I become grid independent. In all the iterative

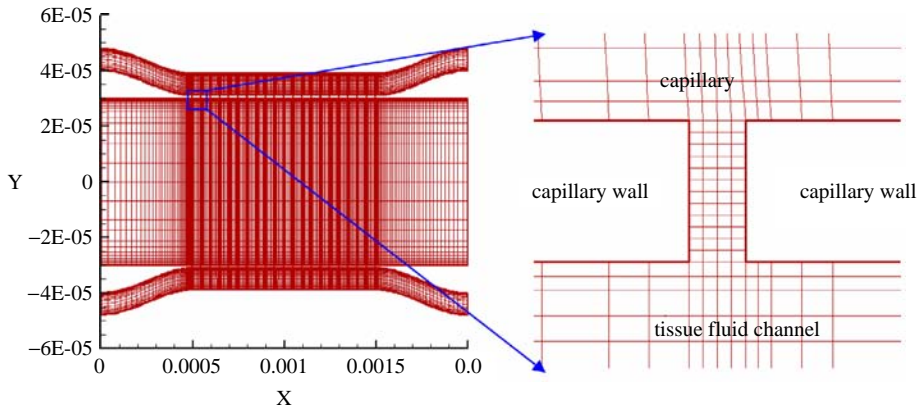


**Figure 5.** The meshes generated for the current electroosmosis flow calculation

processes, calculation of the pressure and velocity values will be terminated when their residual norms become smaller than  $10^{-10}$ .

The wall thickness for capillaries is specified to be  $1\ \mu\text{m}$  with 21 gaps ( $= 0.4\ \mu\text{m}$ ) along a  $1\ \text{mm}$  length. The kinematic viscosities of the tissue fluid and blood flows are assumed to be  $1.2 \times 10^{-3}\ \text{m}^2/\text{s}$  and  $3.0 \times 10^{-3}\ \text{m}^2/\text{s}$ , respectively. The densities of the tissue fluid and blood flows are assumed, respectively, to be  $1,035$  and  $1,057\ \text{kg}/\text{m}^3$ . The capillary flow in the proposed bio-fluid model is of an osmotic type. According to the Starling (1896) equilibrium law, the osmotic velocity depends on the hydraulic (blood hydraulic pressure  $p_{a,v}^*$  and tissue fluid hydraulic pressure  $p_0$ ) and osmotic pressures (plasma osmotic pressure  $\pi_p$  and tissue fluid osmotic pressure  $\pi_0$ ) of the vessel and tissue. Since no coefficient is currently available to represent the osmotic pressure for the blood flows and tissue fluid, the present study considers the simplification by virtue of the expression given by  $p_{a,v} = p_{a,v}^* - \pi_p + \pi_0$ .

The mean values of the body fluid and blood velocities in the investigated tissue fluid channel and capillaries at the arteriole/venule ends are denoted as  $u_t$  ( $u_{t\text{-in}}$  and  $u_{t\text{-out}}$  were the velocities at the inlet and outlet),  $u_a$  and  $u_v$ , respectively. At the normal condition, the hydraulic pressures of arteriole, venule and tissue shown in equation (3) were prescribed as  $p_a^* = 40\ \text{mmHg}$ ,  $p_v^* = 10\ \text{mmHg}$ ,  $p_{0\text{-in}} = 0.03\ \text{mmHg}$ ,  $p_0 = 0\ \text{mmHg}$ , respectively. The osmotic pressures for the plasma and tissue fluids were set to have the values of  $\pi_p = 25\ \text{mmHg}$ ,  $\pi_0 = 5\ \text{mmHg}$ , respectively, (Valtin and Schafer, 1995). In the investigated model, the pressure values for  $p_a$ ,  $p_v$ ,  $p_{0\text{-in}}$  and  $p_0$  are prescribed as  $p_a = 20\ \text{mmHg}$  ( $2,666.44\ \text{nt}/\text{m}^2$ ),  $p_v = -10\ \text{mmHg}$  ( $-1,333.22\ \text{nt}/\text{m}^2$ ),  $p_{0\text{-in}} = 0.03\ \text{mmHg}$

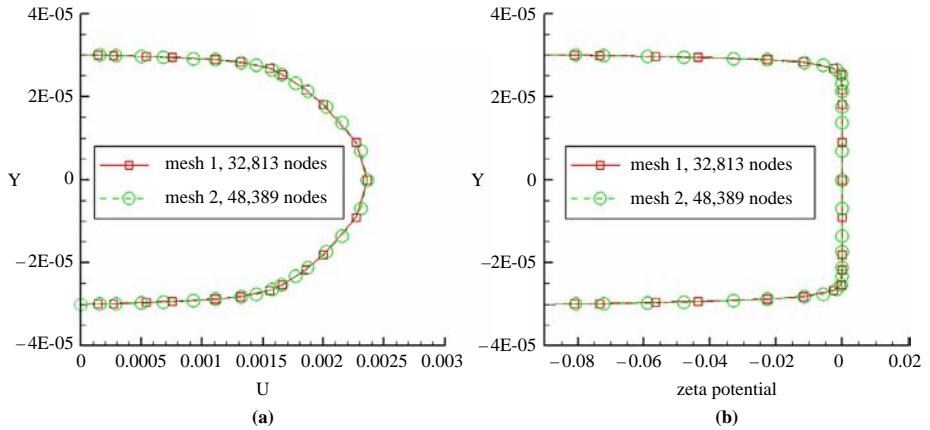


**Figure 6.**  
The predicted grid-independent solutions at  $x = 0.0018\ \text{m}$  in meshes 1 and 2: (a) velocity; (b) zeta potential

**Note:**Tissue fluid channel

**Table I.**  
Check of mass conservation for the calculations carried out in meshes 1 and 2

	Nodal number	$\Delta M/M$
Mesh 1	32,813	$2.11 \times 10^{-2}$ per cent
Mesh 2	48,389	$6.42 \times 10^{-3}$ per cent

**Note:**  $(\Delta M/M) = (M_{\text{in-blood}} + M_{\text{in-tissuefluid}}) - (M_{\text{out-blood}} + M_{\text{out-tissuefluid}}) / (M_{\text{in-blood}} + M_{\text{in-tissuefluid}})$

( $4 \text{ nt/m}^2$ ),  $p_0 = 0 \text{ mmHg}$  ( $0 \text{ nt/m}^2$ ), respectively. The velocity magnitudes for  $u_{t-out}$ ,  $u_a$  and  $u_v$  are predicted to be 4.29, 57.9 and 53.1 cm/min, respectively.

The tissue fluid in the channel under current investigation is rich in ions. In the clinical therapy, the electric paste-piece treatment has been widely employed. To study the resulting electric paste-piece effect, two externally applied potentials  $\phi = 50\text{V}$  and  $\phi = 0\text{V}$  were imposed at the inlet and outlet, respectively. Under the condition of an externally applied voltage, the predicted mean tissue fluid velocities at the electric paste-piece and normal states are compared and tabulated in Table II. The tissue fluid velocity was seen to be increased from 4.29 cm/min to 12.30 cm/min.

The filtration flow from the capillary through 21 gaps to the tissue fluid channel is shown in Figure 7. Since no electric potential gradient is applied in the range between the inlet and outlet gaps, flows passing through the gaps are solely driven by the pressure force. As a result, the velocity profiles are predicted to be similar to each other at the normal and electric paste piece states. In Figure 8, the predicted streamlines are found to be densely distributed downstream of the capillary. The explanation for such distribution is that the tissue flow has been enhanced by the osmosis effect present in

	$U_{0-out}$	Effect of physiology
Normal	4.29 cm/min	At the normal state, the mean velocity of the tissue fluid is about several centimeters per minute
Electric paste piece $V_{ext} = 50\text{V}$	12.30 cm/min (2.86 times of the normal state)	Two electric paste pieces are applied at the upstream and downstream sides of the tissue fluid. The mass transport in the tissue fluid channel becomes faster

**Table II.** Comparison of the predicted velocities for the cases investigated at the normal and electric paste piece states

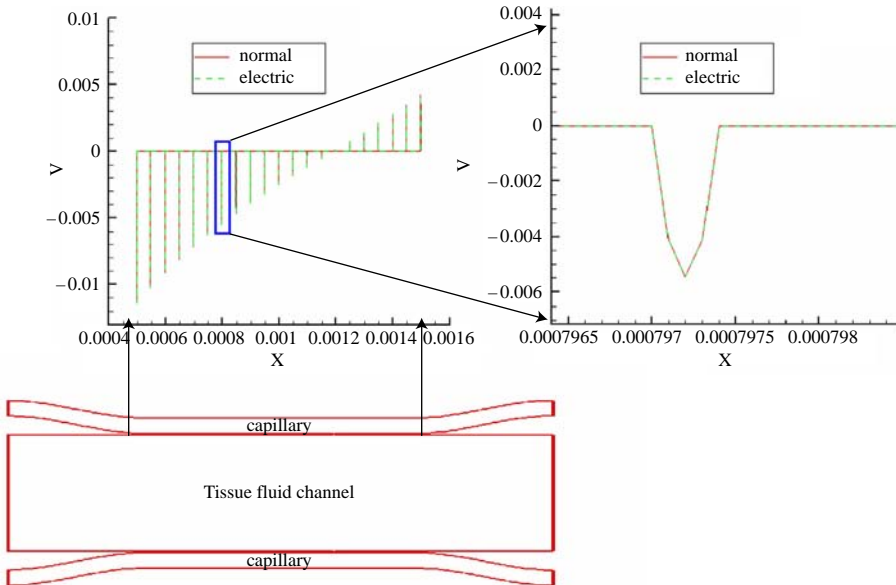
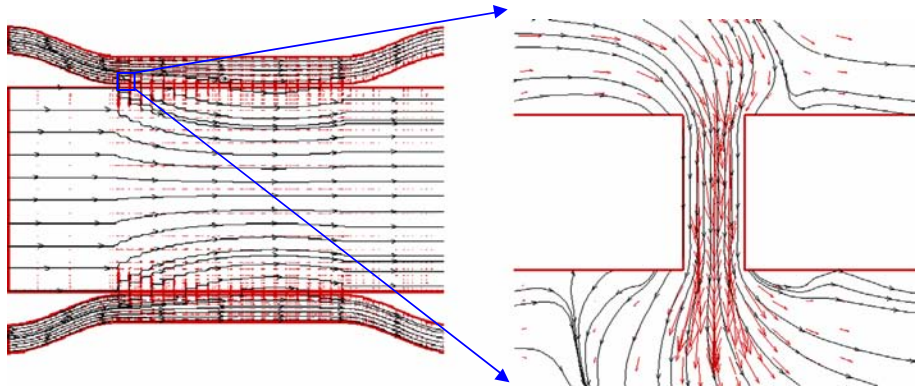


**Figure 7.** The predicted filtration velocity profile along the capillary wall

**Figure 8.**  
The streamlines and velocity vectors predicted at the electric paste piece state

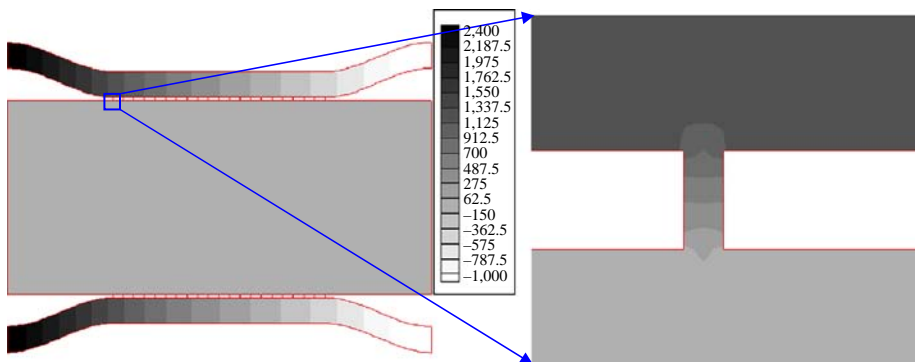


between the plasma and tissue fluids. The predicted velocity vectors along with the predicted pressure contours inside the tissue fluid channel are also shown in Figure 8 for highlighting the osmotic flow behavior. For a pure electroosmotic flow without pressure gradient, the predicted velocity is found to be uniformly distributed in the channel core. Within the EDL region, the flow becomes, however, sharply varied in order to match the no-slip velocity condition at the walls. According to the velocity vectors, the predicted flow is clearly shown to enter the arteriole and exit the venule (outlet). These findings are similar to the theoretical results of Overbeek (1952), Cummings *et al.* (2000) and Santiago (2001).

The predicted contours for both pressure and  $\zeta$  potential are shown in Figures 9 and 10, respectively. It is observed from Figure 9 that the predicted pressures are relatively larger in the arterioles in comparison with those predicted in the venules. Owing to the existence of such a pressure gradient established between the arterioles and venules, there exists a blood flow moving in the direction from the arteriole to the venules. Since the flow can be driven by the pressure and electroosmotic forces, the pressure is distributed fairly uniform in the entire tissue fluid channel and is linearly distributed in the capillaries.

The contours of flow acceleration predicted under the applied electric paste piece and normal states are shown in Figure 11. In the tissue fluid channel, a larger absolute acceleration was found near the capillaries. Fluid flow is accelerated due to filtration in

**Figure 9.**  
The pressure contours predicted at the electric paste piece state



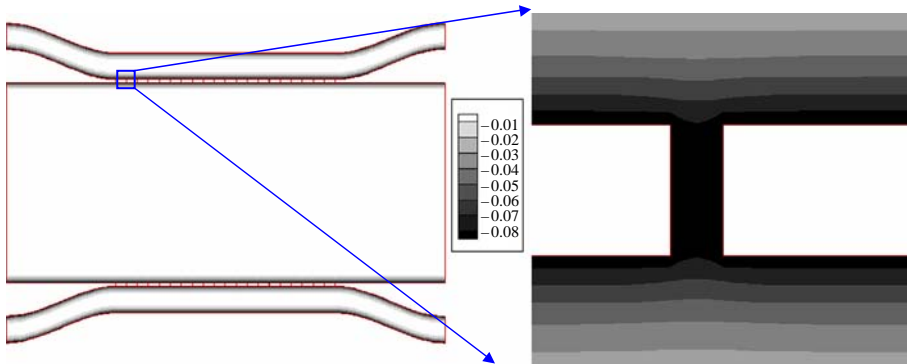


**Figure 10.** The  $\zeta$  potential contours predicted at the electric paste piece state

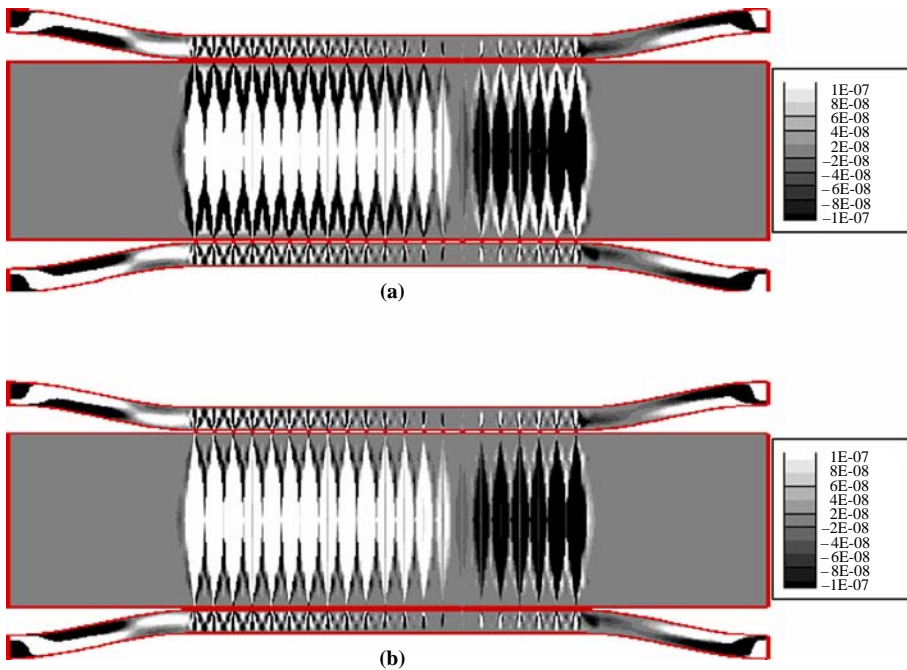


**Figure 11.** The plots of acceleration contours: (a) predicted at the applied electric paste piece state; (b) predicted at the normal state

the range between  $X = 0.0005$  m and  $X = 0.0012$  m and is decelerated in the range between  $X = 0.0012$  m and  $X = 0.0015$  m. By integrating the acceleration values in the tissue fluid channel, the electric paste piece case was found to be able to yield a magnitude of 2.86 times of that predicted under the normal condition. Application of the electric paste piece can, therefore, result in a larger momentum than that predicted at the normal condition owing to the electric force. This phenomenon can be clearly demonstrated from the predicted velocity profiles shown in Figure 12.

Along the line of  $X = 2.2 \times 10^{-4}$  m in the tissue fluid channel, the acceleration value at the normal state is almost zero, as compared with the acceleration value

predicted at the electric paste piece state (Figure 13). According to the computed force components shown in the momentum equation (Figure 14), the tissue fluid channel can be separated into the electric force dominated area (III) and pressure force dominated area (IV). Since the electric force dominated area is predicted to be near the wall, the

**Figure 12.**  
The predicted velocity profiles at  $X = 2.2 \times 10^{-4} \text{ m}$ ,  $6.0 \times 10^{-4} \text{ m}$ ,  $10.1 \times 10^{-4} \text{ m}$  and  $15.3 \times 10^{-4} \text{ m}$ . Note that *N* represents the normal state and *E* denotes the electric paste piece state

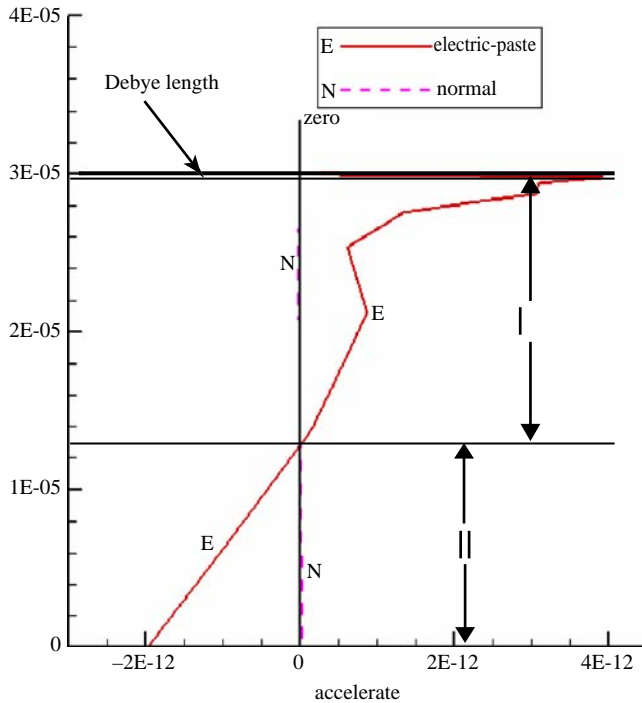
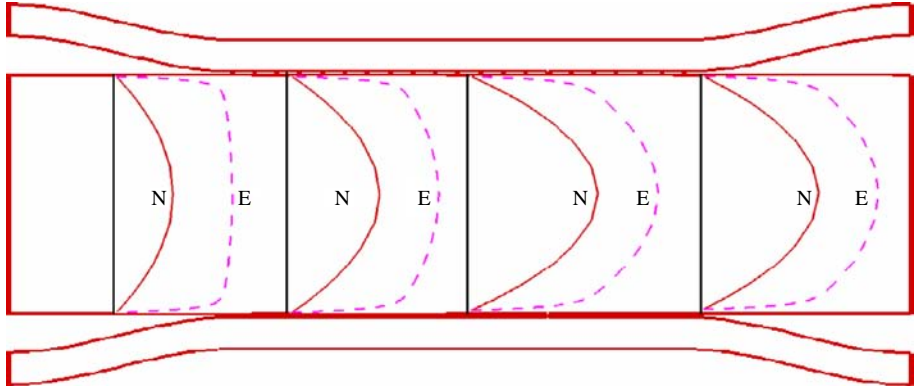


**Figure 13.**  
The predicted flow acceleration at the normal state is almost equal to  $0 \text{ m/s}^2$  along  $X = 2.2 \times 10^{-4} \text{ m}$

**Notes:** At the electric paste piece state, the predicted acceleration can be separated into the (I) acceleration; and (II) deceleration regions

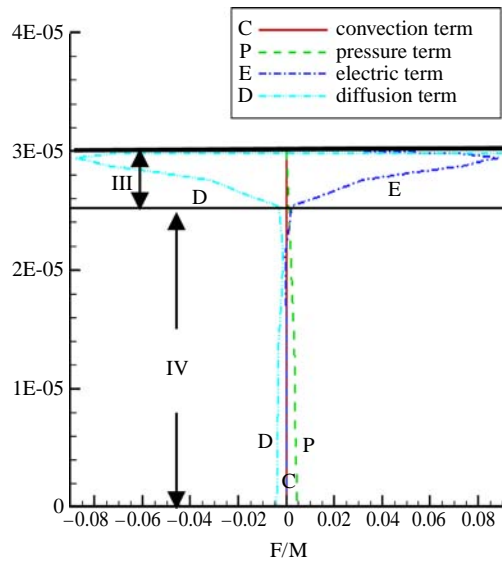
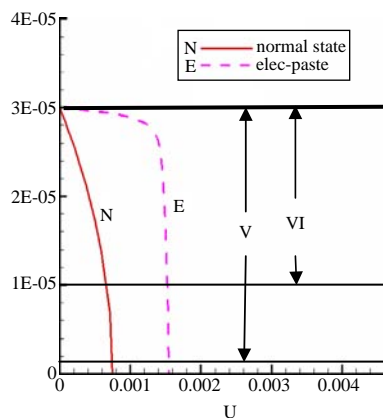


**Figure 14.** At the electric paste piece state, the predicted force components in the momentum equation are separated into the: (III) electric force dominated area; and (IV) pressure force dominated area

electric force can render a larger acceleration (Figure 13) and the velocity profile looks like a plateau (Figure 15) predicted under the electric paste piece state.

### 6. Concluding remarks

The blood and tissue flow motions in the investigated model were considered to be of the creeping type with the respective Reynolds numbers of 0.0106 and 0.0259.



**Notes:** Areas V and VI denote the predicted boundary layers for the cases investigated at the normal and electric paste piece states

**Figure 15.** Comparison of the velocity profiles predicted at the normal and electric paste piece states.

Within the complex electro-osmosis dynamical framework, the Poisson-Boltzmann equation and the modified Navier-Stokes equations are solved together to calculate the electrostatic potential distribution and the blood/tissue fluid velocity in response to the applied electric field with/without the pressure gradient. According to the predicted fluid acceleration, flow rate, and force components shown in the momentum equation, the electric treatment was shown to be able to result in a better curative effect. Furthermore, some dynamic insights of the blood/tissue interaction become more clear through the present study.

### References

- Bensoussan, A. (1991) in Bensoussan, A. (Ed.), *The Nature of Meridians. The Vital Meridian. A Modern Exploration of Acupuncture*, Churchill Livingstone, Edinburgh, p. 51.
- Chang, C.C. and Yang, R.J. (2004), "Computational analysis of electrokinetically driven flow mixing in microchannels with patterned blocks", *Journal of Micromechanics and Microengineering*, Vol. 14, pp. 550-8.
- Chen, X.Y., Toh, K.C. and Yang, C. *et al.* (2004), "Numerical computation of hydrodynamically and thermally developing liquid flow in microchannels with electrokinetics effects", *Journal of Heat Transfer*, Vol. 126, pp. 70-5.
- Cummings, E.B., Griffiths, S.K., Nilson, R.H. and Paul, P.H. (2000), "Conditions for similitude between the fluid velocity and electric field in electroosmotic flow", *Analytical Chemistry*, Vol. 72, pp. 2526-32.
- Debye, P. and Hückel, E. (1923), "Zur Theorie der Elektrolyte", *Physikalische Zeitschrift*, Vol. 24, p. 185.
- Fung, Y.C. (1997), *Biomechanics: Circulation*, Springer, New York, NY.
- Han, J., Zhou, Z. and Xuan, Y. (1983), "Acupuncture has an analgesic effect in rabbits", *Pain*, Vol. 15, pp. 83-91.
- Huang, C., Wang, Y., Han, J.S. and Wan, Y. (2002), "Characteristics of electroacupuncture-induced analgesia in mice: variation with strain, frequency, intensity and opioid involvement", *Brain Research*, Vol. 945, pp. 20-5.
- Jahrul, A. and John, C.B. (2002), "Energy-conserving simulation of incompressible electro-osmotic and pressure-driven flow", *Theoretical and Computational Fluid Dynamics*, Vol. 52, pp. 133-50.
- Ladyshenskaya, O.A. (1969), *The Mathematical Theory of Viscous Incompressible Flow*, 2nd ed., Gordon and Breach, New York, NY.
- Lin, J.Y., Fu, L.M. and Yang, R.J. (2002), "Numerical simulation of electrokinetic focusing in microfluidic chips", *Journal of Micromechanics and Microengineering*, Vol. 12, pp. 955-61.
- Liu, Y.Z., Kim, B.J. and Sung, H.J. (2004), "Two-fluid mixing in a microchannel", *International Journal Numerical Methods Heat Fluid Flow*, Vol. 25, pp. 986-95.
- Mala, G.M., Li, D., Werner, C., Jacobasch, H.J. and Ning, Y.B. (1997), "Flow characteristics of water through a microchannel between two parallel plates with electrokinetic effects", *International Journal Numerical Methods Heat Fluid Flow*, Vol. 18 No. 5, pp. 489-96.
- Mao, W., Ghia, J.N., Scott, D.S., Duncan, G.H. and Gregg, J.M. (1980), "High versus low intensity acupuncture analgesia for treatment of chronic pain: effects on platelet serotonin", *Pain*, Vol. 8, pp. 331-42.
- Overbeek, J.T.G. (1952) in Kruyt, H.R. (Ed.), *Colloid Science*, Elsevier, Amsterdam, p. 1.
- Patankar, N.A. and Hu, H.H. (1998), "Numerical simulation of electroosmotic flow", *Analytical Chemistry*, Vol. 70 No. 9, pp. 1870-81.

- 
- Prashanta, D. and Ali, B. (2001), "Analytical solution of combined electroosmotic/pressure driven flows in two-dimensional straight channels: Finite Debye layer effects", *Analytical Chemistry*, Vol. 73, pp. 1979-86.
- Reuss, F.F. (1809), "Charge-induced flow", *Proceedings of the Imperial Society of Naturalists Moscow*, Vol. 3, pp. 327-44.
- Romita, V.V., Suk, A. and Henry, J.L. (1997), "Parametric studies on electroacupuncture-like stimulation in a rat model: effects of intensity, frequency, and duration of stimulation on antinociception", *Brain Research Bulletin*, Vol. 42, pp. 289-96.
- Santiago, J. (2001), "Electroosmotic flows in microchannels with finite inertial and pressure forces", *Analytical Chemistry*, Vol. 73, pp. 2353-65.
- Sheu, T.W.H. and Chen, H.Y.H. (1999), "A transient analysis of flow in vessels with moving boundaries", *International Journal Numerical Methods Heat Fluid Flow*, Vol. 9 No. 8, pp. 833-46.
- Sheu, T.W.H. and Tsai, S.F. (1999), "A comparison study on fin surfaces in finned-tube heat exchangers", *International Journal Numerical Methods Heat Fluid Flow*, Vol. 9 No. 1, pp. 92-106.
- Sheu, T.W.H., Tsai, S.F. and Wang, M.M.T. (1995), "A Petro-Galerkin formulation for incompressible flows at high Reynolds numbers", *Journal of Computational Fluid Dynamics*, Vol. 5, pp. 213-30.
- Sinton, D., Erickson, D. and Li, D. (2002), "Photo-injection based sample design and electroosmotic transport in microchannels", *Journal of Micromechanics and Microengineering*, Vol. 12, pp. 898-904.
- Starling, E.H. (1896), "On the absorption of fluid from interstitial spaces", *The Journal of Physiology*, Vol. 19, pp. 312-26.
- Stroock, A.D., Dertinger, S.K.W. and Ajdari, A. *et al.* (2002), "Chaotic mixer for microchannels", *Science*, Vol. 295, pp. 647-51.
- Tiberiu, R. and Gheorghe, G. (1981), "Do meridians of acupuncture exist? A radioactive tracer study of the bladder meridian", *American Journal Acupuncture*, Vol. 9-3, p. 251.
- Ulett, G.A., Han, S. and Han, J.S. (1998), "Electroacupuncture: mechanisms and clinical applications", *Biological Psychiatry*, Vol. 44, pp. 129-38.
- Valtin, H. and Schafer, J.A. (1995), *Renal Function*, 3rd ed., Little-Brown, Boston, MA.
- Wan, Y., Wilson, S.G., Han, J. and Mogil, J.S. (2001), "The effect of genotype on sensitivity to electroacupuncture analgesia", *Pain*, Vol. 91, pp. 5-13.
- Wang, M.M.T. and Sheu, T.W.H. (1997), "Implementation of a free boundary condition to Navier-Stokes equations", *International Journal Numerical Methods Heat Fluid Flow*, Vol. 7 No. 1, pp. 95-111.
- Wiedemann, G. (1852), "Über die bewegung im kreise der geschlossenen galvanischen saule", *Progg. Annalen*, Vol. 87, pp. 321-52.

### Further reading

Zhao, J.F. (1997), *Color Atlas of Medical Histology*, Yi-Xuan Press, Taipei.